Effects of heterogeneity on recrystallization kinetics of nanocrystalline copper prepared by dynamic plastic deformation

Lin, Fengxiang; Zhang, Yubin; Tao, Nairong; Pantleon, Wolfgang; Juul Jensen, Dorte

Published in:
Acta Materialia

Link to article, DOI:
10.1016/j.actamat.2014.03.036

Publication date:
2014

Document Version
Publisher's PDF, also known as Version of record

Available online at www.sciencedirect.com

ScienceDirect

Acta Materialia 72 (2014) 252–261

Acta MATERIALIA

www.elsevier.com/locate/actamat

Effects of heterogeneity on recrystallization kinetics of nanocrystalline copper prepared by dynamic plastic deformation

FengXiang Lin [a,*], YuBin Zhang [a], Nairong Tao [b], Wolfgang Pantleon [c], Dorte Juul Jensen [a]

[a] Danish–Chinese Center for Nanometals, Section for Materials Science and Advanced Characterization, Department of Wind Energy, Technical University of Denmark, Risø Campus, 4000 Roskilde, Denmark

[b] Shenyang National Laboratory for Materials Science, Institute of Metal Research, Chinese Academy of Sciences, Shenyang 110016, People's Republic of China

[c] Department of Mechanical Engineering, Section for Materials and Surface Engineering, Technical University of Denmark, 2800 Kongens Lyngby, Denmark

Received 5 February 2014; received in revised form 13 March 2014; accepted 15 March 2014

Abstract

Recrystallization and mechanical behavior of nanocrystalline copper prepared by dynamic plastic deformation (DPD) and DPD with additional cold-rolling (DPD + CR) were investigated, with an emphasis on the effects of heterogeneity within the deformation microstructure. The DPD sample was found to develop a heterogeneous structure, consisting of regions with different textures and microstructures. This heterogeneity within the deformed structure leads to the formation of severely clustered grains in partially recrystallized samples. The recrystallization kinetic curve shows an Avrami exponent less than 1, which is explained using a two-stage kinetics model incorporating the heterogeneity. The heterogeneity of the DPD sample is largely reduced by applying additional rolling. This change in deformation path leads to a more random distribution of the recrystallized grains and more conventional recrystallization kinetics. The hardness of the two samples was measured, and the mechanical properties before and after partial recrystallization of both samples are discussed based on the presence of structural heterogeneities on the macroscopic and the microscopic scale.

Keywords: Nanocrystalline metal; Recrystallization kinetics; Dynamic plastic deformation (DPD); Copper; Mechanical properties

1. Introduction

Nanocrystalline metals with high strength, produced by plastic deformation to large strains, have attracted much research interest over the past decade. Moreover, deformation at high strain rates ($\sim 10^2$–10^3 s^{-1}) can lead to significant structure refinement, even at comparatively low strains, as has been demonstrated by the dynamic plastic deformation (DPD) process [1–4]. DPD is especially effective for structural refinement in copper, since mechanical twinning may become an active deformation mechanism, in addition to dislocation slip [5].

An important issue for nanocrystalline metals is thermal stability, namely whether the original nanostructure can be retained over a period of time at a certain temperature. For nanocrystalline copper produced by severe plastic deformation, recrystallization has been observed to occur even during room temperature storage [6], due to a high stored energy. It is, however, unknown whether the thermal stability can be improved if the initial nanostructure is modified by an additional deformation process. This is investigated in the present work, where deformed and partially recrystallized microstructures as well as the recrystallization kinetics are characterized for two samples, one

* Corresponding author. Tel.: +45 4677 5872; fax: +45 4677 5758.
E-mail address: lnfe@dtu.dk (F. Lin).

http://dx.doi.org/10.1016/j.actamat.2014.03.036
1359-6454/

deformed by DPD to an equivalent strain of $\varepsilon_{vM} = 2.1$ and the other further cold-rolled to $\varepsilon_{vM} = 1.6$ after the DPD process. The aim of the work is to understand how different types of deformation nanostructures affect the recrystallization process and the overall recrystallization kinetics, and thus to study effects of the additional deformation. The recrystallization kinetics is analyzed based on the standard Johnson–Mehl–Avrami–Kolmogorov (JMAK) phase transformation model [7–11]. Moreover, modified versions of this model, which have been developed to incorporate typical microstructural heterogeneity, such as a grain-to-grain variation in the deformation microstructure, have been considered [12,13].

It is known that partial recrystallization typically reduces the strength of nanocrystalline metals, but may improve the ductility. Therefore, thermal annealing has been suggested to be, in some cases, an effective way to optimize the strength–ductility combination [14]. For copper deformed by DPD, it has, however, been found that the ductility does not improve until the recrystallized volume fraction becomes as high as 80% [15], whereas the ductility of the sample with additional rolling can be improved by introducing only a small volume fraction of recrystallized grains [16,17]. These findings are discussed based on the observation that cold-rolling after DPD homogenizes both the deformed and partially recrystallized structures.

2. Experimental

The initial material was 99.995% purity copper with an average grain size of 200 μm (estimated from optical microscopy images, excluding twin boundaries). A cylinder (16 mm in diameter and 26 mm in height) was immersed in liquid nitrogen and processed by DPD through multiple impacts until the height of the sample was reduced to 3.3 mm, which corresponds to an equivalent von Mises strain of 2.1 (defined as $\varepsilon_{vM} = \ln(L_0/L_f)$, where L_0 and L_f are the initial and final height of the sample, respectively). This sample is termed the DPD sample. Experimental details of the DPD process can be found in Ref. [3]. A piece 10 mm in width, 20 mm in length and 3.3 mm in thickness was then cut from the center of the DPD sample, and rolled at room temperature to $\varepsilon_{vM} = 1.6$. The rolling plane coincided with the compression plane during DPD. This sample is termed the DPD + CR sample. It should be noted that both DPD and DPD + CR samples were kept at −18 °C for ~6 months, and at room temperature for some days during transportation from China to Denmark, before they were isothermally annealed and analyzed.

The deformed microstructures were characterized using a Zeiss Supra-35 scanning electron microscope (SEM), equipped with an HKL Channel-5 electron backscatter diffraction (EBSD) system. For the DPD sample, sections from the center of the specimen, perpendicular to the compression plane, parallel to the compression axis (CA), were investigated. For the DPD + CR samples, longitudinal sections, containing the rolling direction (RD) and the normal direction (ND), were characterized. Maps of 60 × 40 μm^2 were obtained using step sizes of 10–50 nm. Since parts of the deformation structure in the DPD sample could still not be resolved due to the very fine structural scale, the present data analysis is supplemented with previous transmission electron microscopy (TEM) results for a similar sample [3]. As shall be described later, it was found that the DPD structure was very heterogeneous, and bigger maps were needed for an overview. These big maps (using a step size of 0.5 μm) were, however, measured after an additional 12 months of storage at −18 °C (i.e. 18 month storage in total). From the big maps, it was observed that the DPD sample was already 18% recrystallized, even though it had never been annealed at elevated temperatures. No recrystallization was, however, observed in the DPD + CR sample. It is unknown when the 18% recrystallization in the DPD sample occurred: during the first or second storage at −18 °C, during the transportation from China to Denmark or during sample preparation for EBSD characterization. Effects of this partial recrystallization of the DPD sample are incorporated in the following analysis, but for simplicity in the following the sample will be termed as-deformed.

The DPD and DPD + CR samples were annealed isothermally at 120 °C and 140 °C, respectively. The annealing temperatures were chosen to enable almost complete recrystallization after annealing for 4 h (14,400 s). The microstructures of the partially recrystallized samples were characterized by EBSD in the same sections as the deformed ones using a step size of 0.5 μm. Recrystallized grains were identified from EBSD orientation data using a Matlab algorithm [18]. Three criteria were applied: (1) pixels inside a recrystallized grain must have pixel-to-pixel misorientations lower than 1°, (2) the equivalent circular diameter (ECD) of the recrystallized grain must be larger than 1.5 μm, (3) the grain must be at least partially surrounded by high angle boundaries, which are defined as boundaries with misorientations higher than 15°. Annealing twins were considered as part of parent grains and twin boundaries were thus ignored in calculation of grain sizes and in visualization of the grains. The recrystallized volume fraction (V_V) was calculated for each annealing duration as the area fraction of recrystallized grains in the measured maps.

Vickers hardness was measured for the as-deformed samples and for samples annealed for 600 s, along a line parallel to the compression direction/ND through the entire sample thickness, on the sections used for EBSD characterizations, using a load of 10 g. The sizes of the hardness indentations were measured not only by optical microscopy but also by SEM using electron channeling contrast (ECC) to determine the diagonal lengths more accurately. Microstructures around the indentations were further characterized by EBSD.

3. Results

3.1. Deformation microstructure of the DPD sample

Fig. 1a shows an orientation map of the DPD sample. Although many pixels could not be indexed by EBSD, the map still represents a structure with regions of different orientations and microstructural characteristics. The green regions (termed Type A structure) in the map are regions of a ⟨1 1 0⟩ fiber texture. The deformation structure of Type A regions is dominated by low angle dislocation boundaries. According to the TEM analysis of Li et al. [3], Type A structure appears to develop by dislocation slip. The blue regions in Fig. 1a (termed Type B structure) are regions of a ⟨1 1 1⟩ fiber texture. The Type B structure is composed of lamellae, with lamellar boundaries almost parallel to the compression plane. Most of the lamellar boundaries are twin boundaries. The Type B structure observed by EBSD can well be regarded as twin bundle regions observed by TEM [3]. It should be noted that the twin boundary spacing in Fig. 1a (~500 nm) is much larger than that obtained from the TEM analysis (10–150 nm). This difference is due to both the limited spatial resolution of EBSD and the scanning step size utilized. All the poorly indexed regions in Fig. 1a are grouped into the so-called Type C structure. In the previous TEM investigations [3], besides regions obviously deformed by dislocation slip and twin bundle regions, fragmented twin bundle regions and shear band regions were observed, both with highly subdivided microstructures (average boundary spacing of 50 nm and 75 nm, respectively). It is suggested that at least a large fraction of the present Type C regions originates from fragmented twin bundles and shear bands.

The quality of the EBSD map shown in Fig. 1a is not sufficient for calculating local stored energy [19]. Instead, the band contrast determined by EBSD is considered as an indicator of the stored energy [20], where a low band contrast value corresponds to a high stored energy, although the stored energy cannot be determined quantitatively. As shown in Fig. 1b, Type A and B structures have much lower stored energies than Type C. This agrees well with previous estimations based on TEM characterization, which reported that the stored energy for the Type A structure was 0.83 J g^{-1}, while that for the Type C structure was 1.60–2.17 J g^{-1} [21]. The stored energy of Type B microstructure is not given in Ref. [21].

It is important to point out that Fig. 1 is a selected example of a small sample area showing all three types of structures (A, B, C) in one map. When larger sample areas are studied, coarse scale heterogeneity is observed, as shown in the sketch in Fig. 2, which is based on six EBSD maps, each covering an area of 250 × 150 μm^2. The structure of the DPD sample is dominated by broad bands of Type A and Type C structures. Within bands of Type A structure, Type C regions appear as long and thin bands (~5 μm in width), which are inclined about 0–20° to the compression plane. Within bands of Type C structure, Type A regions appear as small islands (<20 μm in width). As discussed in Section 2, this as-deformed DPD sample was already 18% recrystallized and the recrystallized regions are sketched in gray in Fig. 2. The remaining Types A and C regions cover 36% and 41% of the total area, respectively, i.e. the ratio between them is ~0.9. The

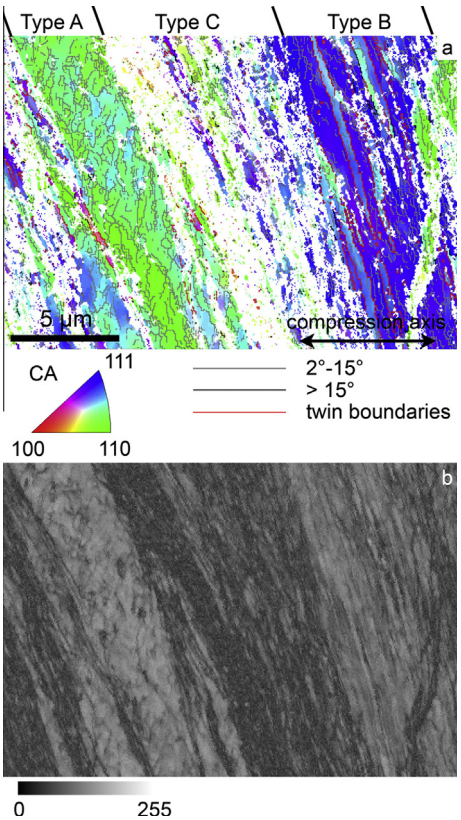

Fig. 1. EBSD data for the as-deformed DPD sample. (a) Orientation map of the deformation structure of the DPD sample viewed in the sample cross-section. The colors represent the crystallographic direction of the compression axis (CA). Non-indexed points are shown in white. Three different types of structure are marked as Types A, B and C, which represent structure dominated by low angle dislocation boundaries, twin bundles and highly fragmented structure, respectively. It should be noted that the fraction of Type B structure is untypically large in this map. (b) Band contrast map of the same area as shown in (a).

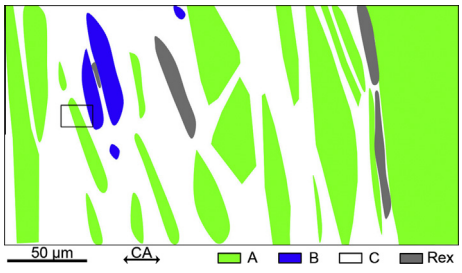

Fig. 2. Sketch of the deformation structure within a large area of the DPD sample, revealing the heterogeneity of the structure. Recrystallization has occurred at the time of the characterization. The recrystallized regions, which normally consist of many recrystallized grains, are marked in gray. The frame marks a region where Fig. 1 may be obtained.

fraction of Type B regions is small; they always appear as islands (<20 μm in width) inside bands of Type C structure. Type B regions occupy only 5% of the total area and will therefore not be discussed further in this paper.

3.2. Deformation microstructure of the DPD+CR sample

The DPD + CR sample has a lamellar structure, with lamellar boundaries aligned along the RD (see Fig. 3a). The Type A and C structures in the DPD sample vanish after additional rolling. A weak rolling texture is developed in this sample, with 36% volume fraction of rolling texture components (copper, S and brass, within 15° deviation from the ideal orientations). Compared with the DPD sample, the DPD + CR sample is much more homogeneous, and Fig. 3a represents well the microstructure of larger areas. Moreover, the large variation in stored energy across different regions seen in the DPD sample has been reduced significantly by cold-rolling, as demonstrated by the band contrast map in Fig. 3b.

3.3. Recrystallization of the DPD sample

Fig. 4a and b shows the microstructure at the initial stage of recrystallization after 300 s of annealing. The recrystallized grains are observed to be clustered. Locally, the recrystallized grains form bands at an angle of 0–20° to the compression plane. They already impinge upon each other inside the bands at this early stage of recrystallization. On the macroscopic scale, the recrystallized volume fraction V_V in the left part of Fig. 4a and b is much higher than that in the right part (0.18 and 0.03, respectively), indicating a coarse scale heterogeneous distribution.

After annealing for 3600 s, almost no Type C regions (highly fragmented structure) remain in the deformed matrix (Fig. 4c). In other words, the large Type C regions have been consumed by recrystallized grains, which are observed in broad recrystallized bands, such as the three bands in Fig. 4c and d. In contrast, large Type A regions (structure dominated by low angle dislocation boundaries), with only few recrystallized grains inside, still exist.

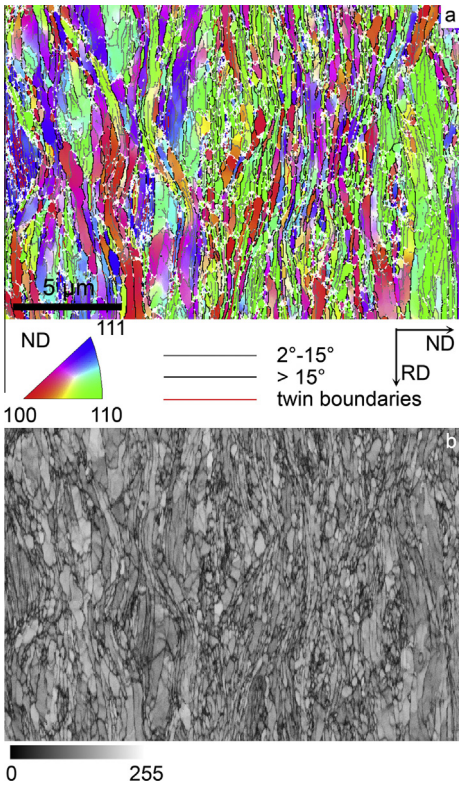

Fig. 3. EBSD data for the as-deformed DPD + CR sample. (a) Orientation map of the deformation structure of the DPD + CR sample viewed in the longitudinal section. The colors represent the crystallographic direction of the normal direction (ND). (b) Band contrast map of the same area as in (a).

3.4. Recrystallization of the DPD + CR sample

At the initial stage of recrystallization (Fig. 5a and b), many small recrystallized grains develop in the DPD + CR samples. They tend to appear within thin bands parallel to the RD, but impingement between the recrystallized grains is not significant. In Fig. 5b, 42% of the recrystallized grains have boundaries fully surrounded by deformed matrix (this fraction is only 12% for the DPD sample shown in the map in Fig. 4b). On the macroscopic scale, the spatial distribution of the recrystallized grains is much more random than that in the DPD sample. As the recrystallization continues (Fig. 5c and d), the recrystallized grains impinge upon each other mainly along RD, whereas the impingement along ND is much less significant.

3.5. Kinetics

The recrystallized volume fraction V_V as a function of annealing time t is shown in Fig. 6a. For the DPD sample, the measured recrystallized volume fractions from different EBSD maps ($150 \times 250\ \mu m^2$ each) for the same sample show a large spread. For example, for the seven maps measured for the DPD sample annealed for 120 s, the minimum V_V is 0.02, whereas the maximum is 0.69. For the DPD + CR sample, the recrystallized volume fractions measured in different locations are quite similar.

The evolution of V_V with t is often expressed by the JMAK equation [7–11]:

$$V_V = 1 - \exp(-kt^n) \quad (1)$$

The exponent n in Eq. (1) can be derived from the slope of the so-called Avrami plots, i.e. plots of $-\ln(1 - V_V)$ as a function of t on a log–log scale. Fig. 6b shows the Avrami plots of the DPD and DPD + CR samples using the average V_V for each annealing duration. For the DPD + CR sample, the exponent n is 1.06, if all the data points are included in the fitting. The point for the longest annealing time $t = 14{,}400$ s has an obvious deviation towards lower values from the fitted line, which has been seen previously in rolled copper [22]. If this point is excluded from the

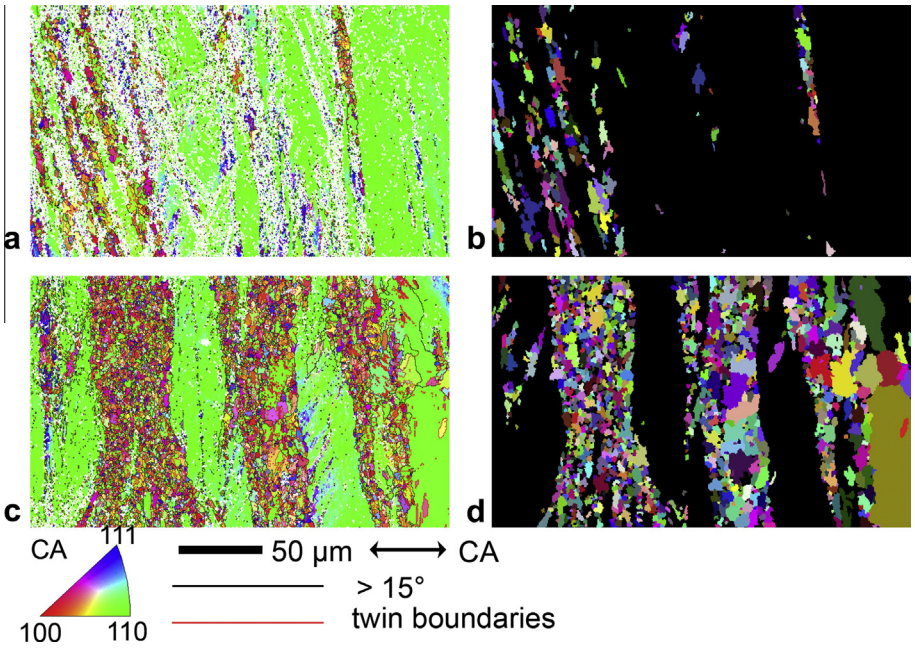

Fig. 4. Orientation maps of partially recrystallized microstructures of the DPD sample annealed at 120 °C for 300 s (a) and 3600 s (c). Maps shown in (b and d) highlight the recrystallized grains in random colors. Each grain and all its twin parts are shown in the same color. Non-recrystallized regions are shown in black.

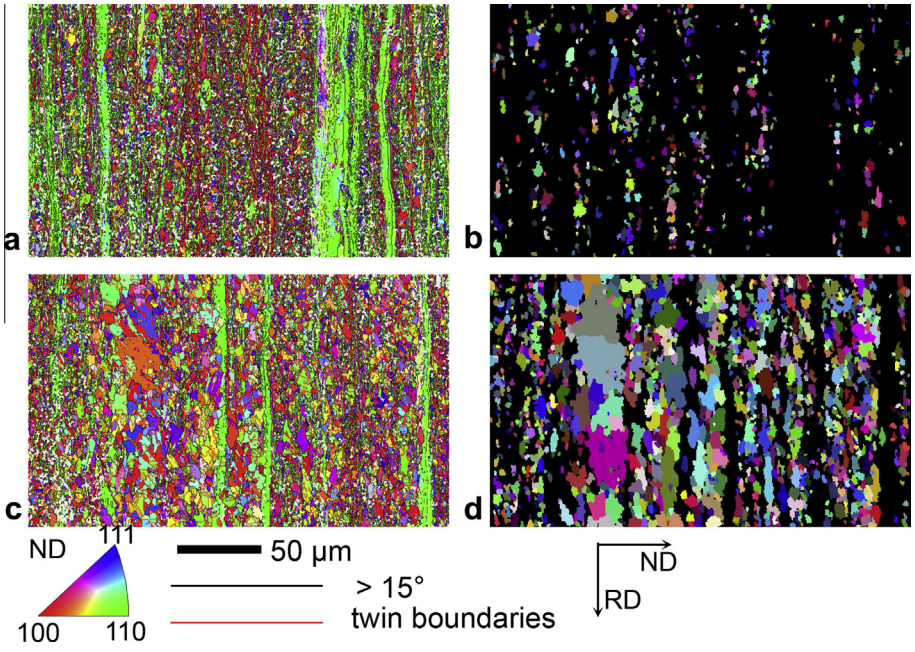

Fig. 5. Orientation maps of partially recrystallized microstructures of the DPD + CR sample annealed at 140 °C for 1200 s (a) and 3600 s (c). Maps shown in (b and d) highlight the recrystallized grains in random colors. Each grain and all its twin parts are shown in the same color. Non-recrystallized regions are shown in black.

fitting, an exponent of 1.57 is obtained. For the DPD sample, the data points fit to a straight line for the whole annealing period, but a very low exponent $n = 0.37$ is found.

As mentioned in the experimental part, for the samples stored for 18 months, no recrystallization occurred in the DPD + CR sample, whereas 18% of the material was recrystallized in the DPD sample. Therefore, the isothermal kinetics of the DPD sample needs correction. The measured V_V for the DPD sample can be corrected for the already recrystallized volume as follows:

$$V'_V = (V_V - V_{V,0})/(1 - V_{V,0}) \quad (2)$$

where $V_{V,0}$ is the recrystallized volume fraction after storage. With this correction, we are only considering the kinetics of the matrix, which was not recrystallized before

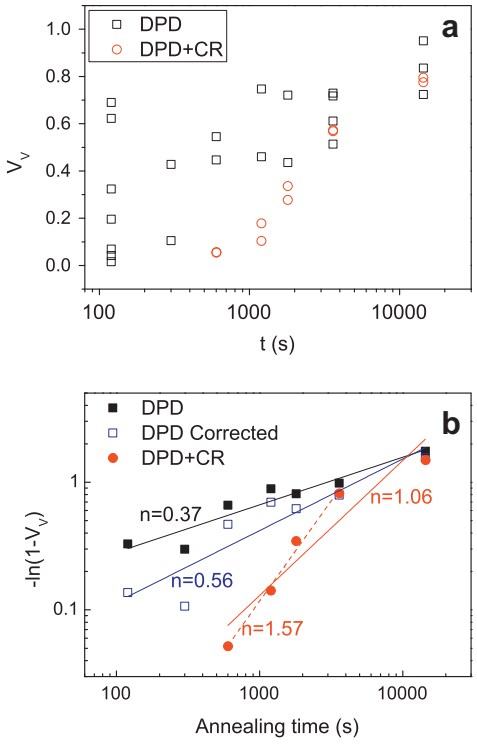

Fig. 6. Time dependence of recrystallized volume fraction for the DPD and the DPD + CR samples. (a) Recrystallized volume fraction V_V as a function of annealing time t. Each point represents the V_V measured from one EBSD map ($250 \times 150\ \mu m^2$). For each sample, 2–7 maps were measured. Note that for the DPD + CR sample, the two data points for 300 s annealing coincide, which is also the case for 3600 s annealing. (b) Avrami plots of the average V_V for each annealing duration. The open squares represent the corrected recrystallized volume fraction V'_V using Eq. (2). Each set of data is fitted by a straight line, where the slope represents the exponent n in Eq. (1). For the DPD + CR sample, an extra fitting to the first four points was made to get a better match between the experimental data points and the fitted line.

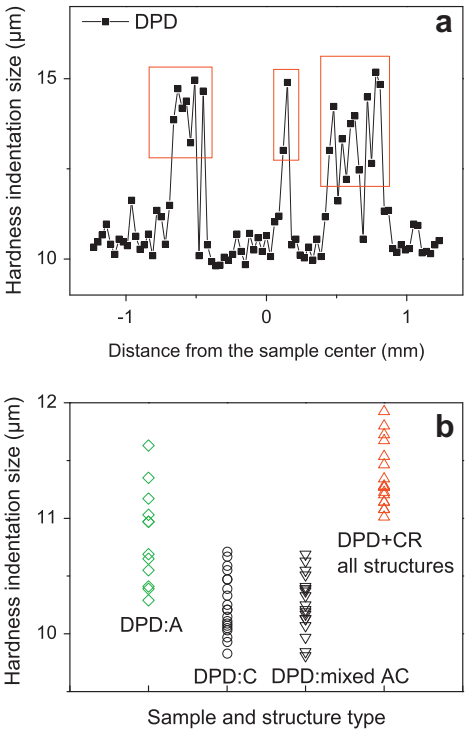

Fig. 7. Hardness for the as-deformed DPD and DPD + CR samples. (a) Variation in hardness indentation size along a line parallel to the compression direction through the sample thickness, for the as-deformed DPD sample. The size is calculated as the average length of the two diagonals of each hardness indentation. (b) Sizes of hardness indentations in different types of structures of the as-deformed DPD sample. The sizes of hardness indentations in the as-deformed DPD + CR sample are also shown.

furnace annealing. Although the $V_{V,0}$ of the series of isothermal samples (6 month storage) is unknown, it may be conservatively assumed to be 18% (the value observed after 18 month storage). The Avrami exponent for the DPD sample of the corrected V'_V now equals 0.56 (see Fig. 6b), which is still rather low.

3.6. Hardness

To ease the interpretation of the observed recrystallization results and to link these to the mechanical properties, a series of hardness measurements were performed in both the as-deformed and partially recrystallized (after 600 s annealing) DPD and DPD + CR samples along lines through the thickness of the samples. The result for one such line of hardness indentations in the as-deformed DPD sample is shown in Fig. 7a. Some of the indentions (marked by frames in Fig. 7a) are clearly larger than the others and originate from regions which were recrystallized during the 18 month storage. In the following, only indentations in the deformed matrix (as verified by ECC images) are considered. For all these indentations in the deformed matrix, the orientations of the surrounding regions were determined by EBSD. In some cases both Type A structure (structure dominated by low angle dislocation boundaries) and Type C structure (highly fragmented structure) are observed near the indentation (which in the following are referred to as from mixed AC regions), but in many cases an indentation is fully surrounded by either Type A or Type C structure.

The sizes of the indentations measured in the as-deformed DPD sample are presented in Fig. 7b, which show a large spread from 9.8 μm to 11.6 μm, corresponding to a hardness spread from 193 kgf mm^{-2} to 137 kgf mm^{-2}. Although the sizes of indentations in Type A and C regions have some overlap, indentations in Type A regions are in general larger than those in Type C regions. The sizes of indentations in mixed AC regions are similar to those in Type C regions. The corresponding hardness is given in Table 1.

For the DPD sample annealed for 600 s at 120 °C, hardness indentations measured in the remaining deformed matrix are mainly from Type A regions, since after annealing, large Type C regions are rare. The hardness of this remaining deformed matrix is reduced by 6% (see Table 1), compared with that of Type A regions before annealing, which implies some static recovery.

Table 1
Vickers hardness for the as-deformed and partially recrystallized DPD and DPD + CR samples.

Sample	Type A regions (kgf mm^{-2})	Type C regions (kgf mm^{-2})	Mixed AC regions (kgf mm^{-2})	Average for the deformed matrix (kgf mm^{-2})
DPD as-deformed	158 ± 11	177 ± 9	176 ± 8	172 ± 12
DPD 600 s at 120 °C	148 ± 10	–	–	148 ± 10
DPD + CR as deformed	–	–	–	144 ± 7
DPD + CR 600 s at 140 °C	–	–	–	132 ± 10

For the as-deformed DPD + CR sample, the sizes of the indentations vary from 11.0 μm to 11.9 μm (see Fig. 7b), and the spread of these indentation sizes is thus much smaller than in the entire DPD sample. After 600 s of annealing, the hardness of the deformed matrix in the DPD + CR sample decreases by 8%, compared with that in the as-deformed DPD + CR sample (see Table 1), again due to static recovery.

4. Discussion

4.1. Origin of heterogeneity of the DPD sample

An important feature of the as-deformed DPD sample is the existence of regions of different structures, which are distributed heterogeneously on a rather coarse scale (~100 μm). Although previous TEM investigations have suggested that the DPD sample consists of several types of microstructures [3], the coarse scale heterogeneous distribution has not been discussed in Ref. [3] probably due to the limited observation area available for individual TEM specimens. EBSD, in contrast, allows characterization of a large area, and in spite of loss of microstructural details, EBSD gives a good fingerprint of the heterogeneity of the sample.

The heterogeneous deformation structure of the DPD sample seems to be directly related to the coarse grain size (~200 μm) of the initial sample before DPD deformation. Clear indications of this are given by the microstructure of the same sample deformed by DPD to a lower strain ($\varepsilon_{vM} = 0.4$), which is shown in Fig. 8. The initial grain boundaries can still be recognized in this map. The microstructure shows large variations between grains. Some grains deform by dislocation slip, while other grains deform by twinning. The deformation mechanisms in different grains depend on the grain orientation, as has been pointed out for this material by Hong et al. [23]. It is important to note that grains with a ⟨1 1 0⟩ fiber texture (the green grains in the map) deform fairly homogeneously, which is in agreement with previous results for compressed copper [24], and which may be related to the stability of such orientations during compression. It is thus suggested that each large Type A region (structure dominated by low angle dislocation boundaries) in the DPD ($\varepsilon_{vM} = 2.1$) sample originates from an individual grain with an initial orientation close to the ⟨1 1 0⟩ fiber texture. Further support for this suggestion is that the size of individual Type A regions corresponds well with the initial grain size (as grains of 200 μm size deformed to a strain of 2.1 should flatten to 25 μm). Twinning occurs more often in grains with initial orientations away from the ⟨1 1 0⟩ fiber texture. During further deformation, twin planes in these grains have been described to rotate gradually towards the compression plane [25]. At the same time, the twin lamellae become fragmented by dislocations accumulated in the twin boundaries and by shear bands [26]. Except for a few less fragmented parts, which contribute to Type B structure (twin bundles), most of these initial grains may contribute to Type C structure (highly fragmented structure) in the DPD ($\varepsilon_{vM} = 2.1$) sample.

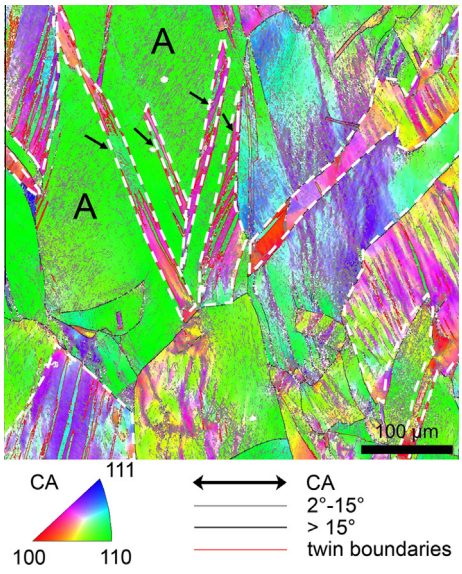

Fig. 8. Orientation map of the microstructure of a sample deformed by DPD to $\varepsilon_{vM} = 0.4$. Areas showing a high frequency of deformation twins are outlined by white dashed lines. One grain (marked as Grain A) deforms most likely by dislocation slip, while deformation twinning occurs in its annealing twins (marked by arrows).

4.2. Two-stage kinetics model

The classical JMAK recrystallization kinetics model is based on the assumption that the nucleation sites are randomly distributed and that all grains grow at the same growth rate. For a constant growth rate, the JMAK model predicts an exponent n of 3 and 4 for three-dimensional (3-D) growth, assuming site-saturated nucleation and a

constant nucleation rate, respectively. This model is, however, too simplified to describe most recrystallization processes, despite that Eq. (1) often fits the experimental data points well (e.g. [27]). Some modified kinetics models have been suggested (e.g. [28–30]), which consider effects of non-random nucleation, and variation of growth rates with time and/or with orientations. These modified models lead to an Avrami exponent lower than 3–4, and can explain the deviation to lower values towards the end of recrystallization, as observed in the DPD + CR sample. However, an exponent as low as that for the DPD sample ($n = 0.56$) has not been reported, and to our knowledge, no models can describe such kinetics reasonably.

For the DPD sample, the heterogeneity within the deformed matrix is essential. Type C regions (highly fragmented structure) recrystallize much more readily than Type A regions (structure dominated by low angle dislocation boundaries). For modeling the overall kinetics, these different regions need to be treated independently. In this work, we thus consider a sample consisting of two distinct regions: fast recrystallizing regions (FRRs) and slowly recrystallizing regions (SRRs), each with their own recrystallization kinetics given as

$$V_{V,i} = 1 - \exp(-k_i t^{n_i}) \tag{3}$$

where i represents either fast or slowly recrystallizing regions. By further assuming that recrystallized grains grow separately within either FRRs or SRRs, which is largely substantiated by the observed partially recrystallized structure (see Fig. 4), the overall kinetics can then be expressed as:

$$\begin{aligned} V_V &= XV_{V,F} + (1-X)V_{V,S} \\ &= X(1 - \exp(-k_F t^{n_F})) + (1-X)(1 - \exp(-k_S t^{n_S})) \end{aligned} \tag{4}$$

where X is the volume fraction of the FRRs and the subscripts F and S represent fast and slowly, respectively.

An estimation of n_i representative for the fast and slowly recrystallizing regions is not directly possible from the present experimental data. The value of n_i depends on the nucleation and growth condition within each region. As has been suggested in many experimental researches (e.g. Ref. [12]), the theoretical value of 3–4 is rarely observed for recrystallization of most materials. In the present work, we have chosen to set n_i in Eq. (4) to be 1, because this is typical for pure copper samples (which do not develop large scale heterogeneity) deformed to various strains [12], including the present DPD + CR sample. In this case, Eq. (4) can be rewritten as

$$V_V = X(1 - \exp(-k_F t)) + (1-X)(1 - \exp(-k_S t)) \tag{5}$$

In an Avrami plot, a kinetic curve given by Eq. (5) will at the beginning (for short annealing times) follow the line of the FRRs, while at the end it follows that of the SRRs, each with a slope close to 1. At intermediate stages, a transition region with a much lower slope can be observed.

By fitting the experimental data for the DPD sample using Eq. (5), the curve in Fig. 9 is obtained. It is seen that the overall curve shown in Fig. 9 describes the experimental data well. The fitted value for X, k_F and k_S are 0.48, $1.9 \times 10^{-3}\ s^{-1}$ and $6.5 \times 10^{-5}\ s^{-1}$, respectively, giving a ratio k_F/k_S of 29. These fitted values can be compared to values obtained directly from the experiments. As Type A and Type C regions can be considered as SRRs and FRRs, respectively, $(1-X)/X$ should then match the ratio between the volume fraction of A and C. The fitted value X gives a ratio $(1-X)/X$ of 1.1, and this ratio is not far from the experimental value of 0.9. The experimental k_F/k_S ratio may be estimated based on the growth rates of grains within Type C and A regions. If we assume $v = M \cdot F$ and the mobility M is similar in both regions, the difference in stored energy F, which according to the calculations by Yan and Zhang [21] is 0.83 J g^{-1} for Type A, and 1.60–2.17 J g^{-1} for Type C, i.e. in the range of 2–3 times, directly determines the differences in linear growth rates v. For the present sample a constant average aspect ratio of the recrystallized grains is observed, indicating a 3-D growth. It should be noted that for a growth rate decreasing with time, 3-D growth is not in conflict with an Avrami exponent of 1. Assuming such 3-D growth, a factor of 2–3 in the linear growth rates corresponds to a k_F/k_S ratio of 2^3–3^3 times, i.e. 8–27 times. Higher values in this range agree well with the k_F/k_S ratio of 29 determined from the model. It should be noted that different nucleation rates are not considered in this estimation, and the k_F/k_S ratio may thus tend to be underestimated. In general, despite the simple nature of the model, it not only gives a good fit to the experimental data, but also provides fitted parameters that can be experimentally substantiated. Previously, this type of model was used [12,13] to explain the occurrence of effective Avrami exponents lower than the theoretical values 3 or 4 by a combination of different kinetics each with a theoretical exponent. Here, a combination of local kinetics with already low exponents is utilized to rationalize exponents even lower than 1.

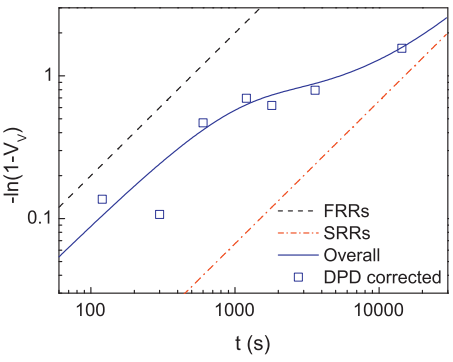

Fig. 9. Avrami plot of the DPD sample fitted using Eq. (5). The sample is assumed to consist of two distinct regions, namely FRRs and SRRs, and each region recrystallizes with a kinetics exponent $n = 1$, which is typical for many metals and has been observed for the present DPD + CR sample.

4.3. Effects of heterogeneity on mechanical properties

It is interesting to note that the DPD and the DPD + CR samples have quite different mechanical properties and that partial recrystallization affects the uniform elongation differently in the two types of samples [15–17]. The yield strengths ($\sigma_{0.2\%}$) of fresh (i.e. without storage) DPD and DPD + CR samples have previously been reported to be 585 MPa and 485 MPa, respectively [15,31]. These values may be compared to the hardness values measured in the present work using $\sigma_{0.2\%} = HV/3$ [32]. The average hardness values, which are 172 kgf mm^{-2} for the DPD sample and 144 kgf mm^{-2} for the DPD + CR sample, convert to $\sigma_{0.2\%}$ of 562 MPa and 470 MPa, respectively. Hence, the estimated $\sigma_{0.2\%}$ of the two samples corresponds well with the measured ones. The yield stress of the DPD + CR sample is lower than that of the DPD sample, which indicates an overall decrease in stored energy. This behavior is interesting as the total plastic strain is significantly larger in the DPD + CR sample. Tentatively, it is suggested that the change in deformation path leads to changes in the active slip systems and to reorganization of the deformation microstructure. This may lead to dynamic recovery, reducing the dislocation content and also reducing the yield stress and the stored energy. Therefore the additional cold-rolling reduces the driving force for recrystallization and thus increases the thermal stability of the sample.

The introduction of recrystallized grains into the nanocrystalline matrix (to create a "composite" structure) has been suggested as a possible way to increase the ductility [14]. However, the "efficiency" of recrystallized grains for improving ductility may be significantly different. This is clearly seen in the DPD and DPD + CR samples investigated in this study. Before recrystallization, the uniform elongation was 1% and 4.5% for the DPD and DPD + CR samples, respectively [15,31]. Partial recrystallization of the DPD sample has been shown to have limited effects on the uniform elongation, even for high V_V [15]. This is in strong contrast to the results of the DPD + CR sample, for which the uniform elongation increases linearly with V_V [16,17]. It thus appears that the ductility of the partially recrystallized samples is also affected by other parameters.

For the DPD and DPD + CR samples with a similar recrystallized volume fraction, ductility can be quite different. For example, for the ~60% recrystallized samples, the uniform elongation is 1% for the DPD sample and 15% for the DPD + CR sample. Nevertheless, the average sizes (ECDs) of recrystallized grains are ~4 μm in both samples. The grain size distribution is plotted in Fig 10. Both distributions peak at ~5 μm. The two distributions are similar, except that the size distribution of the DPD sample has a longer tail. However, grains larger than 30 μm only occupy 5% of the total area in the DPD sample. Therefore, the different elongation is not due to the difference in sizes of the recrystallized grains.

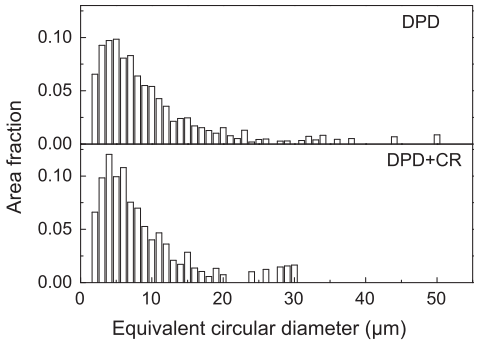

Fig. 10. Area-weighted size distributions of recrystallized grains for samples approximately 60% recrystallized. For the DPD sample, four annealing durations (600 s, 1200 s, 1800 s and 3600 s at 120 °C) are included, all with recrystallized volume fractions ~60% (see also Fig. 6a). The DPD + CR sample was annealed at 140 °C for 3600 s.

A significant difference between the DPD and DPD + CR samples is the heterogeneity within the samples, in both the deformed and the partially recrystallized state. In the DPD sample the deformation microstructure is heterogeneous, consisting of broad bands with different microstructural characteristics (and therefore stored energies), and the recrystallized grains are severely clustered in broad bands. On the contrary, the change in deformation path in the DPD + CR sample leads to a more homogeneous deformation microstructure and spatially more randomly distributed recrystallized grains. It is also observed that the hardness variation within the deformation structure is reduced after additional cold-rolling (comparing the hardness indentation size spreads in Fig. 7b for the DPD and DPD + CR samples). This means that the strain distribution during tensile testing will be more uniform in the DPD + CR sample and stress build-up at hard areas will be reduced (e.g. [33]). As a result, ductility in general will be improved – as observed.

5. Conclusions

1. The deformation structure of the DPD sample is very heterogeneous, which is interpreted as effects of the orientations and the large sizes of the initial grains before deformation. The course of the recrystallization reflects the deformation heterogeneity: the high stored energy regions (highly fragmented structure including fragmented twin bundles and shear bands, termed Type C) recrystallize first and recrystallization may occur even during low temperature storage, whereas low stored energy regions (structure dominated by low angle dislocation boundaries, termed Type A) resist recrystallization. Consequently, the recrystallized grains are clustered in broad bands. The heterogeneity of the deformation microstructure also affects the recrystallization kinetics, and leads to a very low Avrami exponent

below 1. A two-stage recrystallization model has been applied, which describes the experimental data satisfactorily.

2. After additional rolling of the DPD sample (the DPD + CR sample), the deformation structure becomes much more homogeneous, and the recrystallized grains are distributed significantly more randomly. The rolling process after DPD has several positive effects. Firstly, it increases the thermal stability of the sample by distributing and lowering the stored energy and thereby retarding recrystallization. Secondly, it decreases the microstructural heterogeneity introduced in the DPD process, leading to a significantly improved ductility in the partially recrystallized samples. The good combination of strength and ductility of DPD + CR samples suggests that it may be helpful to combine several deformation processes in order to optimize both the thermal and mechanical performance of nanocrystalline metals.

Acknowledgements

The authors gratefully acknowledge the support from the Danish National Research Foundation (Grant No. DNRF86-5) and the National Natural Science Foundation of China (Grant No. 51261130091) to the Danish-Chinese Center for Nanometals, within which this work has been performed.

References

[1] Zhao WS, Tao NR, Guo JY, Lu QH, Lu K. Scripta Mater 2005;53:745.
[2] Tao NR, Lu K. J Mater Sci Technol 2007;23:771.
[3] Li YS, Tao NR, Lu K. Acta Mater 2008;56:230.
[4] Luo ZP, Mishin O, Zhang YB, Zhang HW, Lu K. Scripta Mater 2012;66:335.
[5] Christian JW, Mahajan S. Prog Mater Sci 1995;39:1.
[6] Mishin OV, Godfrey A. Metall Mater Trans 2008;39A:2923.
[7] Johnson WA, Mehl RF. Trans AIME 1939;135:416.
[8] Avrami MJ. Chem Phys 1939;7:1103.
[9] Avrami MJ. Chem Phys 1940;8:212.
[10] Avrami MJ. Chem Phys 1941;9:177.
[11] Kolmogorov AN. Izv Akad Nauk USSR Ser Fiz 1937;1:355.
[12] Doherty RD, Rollett AD, Srolovitz DJ. In: Hansen N et al., editors. Annealing processes. Proceeding of the 7th Risø international symposium on metallurgy and materials science. Roskilde: Risø National Laboratory; 1986. p. 53.
[13] Rollett AD, Srolovitz DJ, Doherty RD, Anderson MP. Acta Metall 1989;37:627.
[14] Koch CC. Scripta Mater 2003;49:657.
[15] Li YS, Zhang Y, Tao NR, Lu K. Scripta Mater 2008;59:475.
[16] Zhang Y. Investigations on the strengthening and toughening of bulk nanostructured Cu and Cu–Al alloy. Ph.D. thesis. Institute of Metal Research, Chinese Academy of Science; 2010.
[17] Zhang Y, Tao NR, Lu K. In preparation.
[18] Wu GL, Juul Jensen D. Mater Charact 2008;59:794.
[19] Godfrey A, Cao WQ, Hansen N, Liu Q. Metal Mater Trans 2005;36A:2371.
[20] Gerber Ph, Baudin T, Jakani S, Mathon MH, Bacroix B. Mater Sci Forum 2004;51–56:467.
[21] Yan F, Zhang HW. J Mater Sci Technol 2012;28:289.
[22] Vandermeer RA, Juul Jensen D. Metal Mater Trans 1995;26A:2227.
[23] Hong CS, Tao NR, Lu K, Huang X. Scripta Mater 2009;61:289.
[24] Lee CS, Lee CF, Smallman RE. Texture Microstruct 1996;26–27:137.
[25] Lin FX, Delannay L, Leffers T. In preparation.
[26] Hong CS, Tao NR, Huang X, Lu K. Acta Mater 2010;58:3103.
[27] Vandermeer RA, Rath BB. Metal Trans 1989;20A:391.
[28] Furu T, Marthinsen K, Nes E. Mater Sci Technol 1990;6:1093.
[29] Marthinsen K, Lohne O, Nes E. Acta Metall 1989;37:135.
[30] Marthinsen K, Fridy JM, Rouns TN, Lippert KB, Nes E. Scripta Mater 1998;39:1177.
[31] Zhang Y, Tao NR, Lu K. Acta Mater 2008;56:2429.
[32] Tabor D. Proc Roy Soc Lond A 1948;192:247.
[33] Mattei L, Daniel D, Guiglionda G, Moulin N, Klöcker H, Driver J. Mater Sci Eng A 2013;583:96.